Article

pubs.acs.org/Biomac

Vorinostat–Polymer Conjugate Nanoparticles for Acid-Responsive Delivery and Passive Tumor Targeting

Iza Denis,[†,‡,§] Fatima el Bahhaj,[⊥] Floraine Collette,[∥] Régis Delatouche,[⊥] Fabien Gueugnon,[†,‡,§] Daniel Pouliquen,[†,‡,§] Loic Pichavant,[∥] Valérie Héroguez,[∥] Marc Grégoire,[†,‡,§] Philippe Bertrand,*[,⊥,#] and Christophe Blanquart*[,†,‡,§,#]

[†]Inserm, UMR 892, Nantes F-44000, France

[‡]CNRS, UMR 6299, Nantes F-44000, France

[§]University of Nantes, 8 quai Moncousu, F-44007 Nantes cedex 1, France

[∥]Laboratoire de Chimie des Polymères Organiques, CNRS, UMR 5629, Bordeaux, 16 Avenue Pey-Berland, F-33607 Pessac, France

[⊥]Institut de Chimie des Milieux et Matériaux de Poitiers, CNRS, UMR 7582, Poitiers, 4 rue Jacques Fort, B28, F-86000 Poitiers, France

[#]Réseau Épigénétique du Cancéropôle Grand Ouest, France

Supporting Information

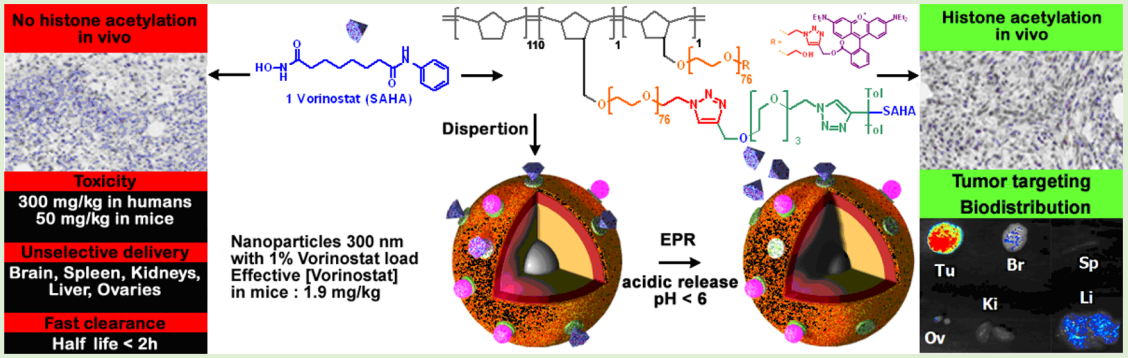

ABSTRACT: In vivo histone deacetylase (HDAC) inhibition by vorinostat under clinically acceptable dosing is limited by its poor pharmacokinetics properties. A new type of nontoxic pH-responsive delivery system has been synthesized by ring-opening metathesis polymerization, allowing for the selective distribution of vorinostat in mesothelioma tumors in vivo and subsequent histone reacetylation. The delivery system is synthesized by generic click chemistry, possesses native stealth properties for passive tumor targeting, and does not need additional chemistry for cellular internalization. Although vorinostat alone at 50 mg/kg in mice showed no effect, our new delivery system with 2 mg/kg vorinostat promoted histone reacetylation in tumors without side effects, demonstrating that our strategy improves the activity of this HDAC inihibitor in vivo.

1. INTRODUCTION

Vorinostat (Figure 1, suberoyl anilide hydroxamic acid) is approved by FDA for the treatment of cutaneous T-cell lymphoma[1] because of its potent activity based on inhibition of the zinc-dependent histone deacetylases (HDAC), one of the epigenetic protein targets overexpressed in cancer cell lines. The HDAC inhibitory effect of vorinostat at micromolar concentrations leads to reacetylation of histones, which, in turn, stimulates tumor suppressor gene expression, inducing differentiation,[2] growth arrest at G1 and G2–M of the cell cycle,[3] or apoptosis. Several clinical trials have investigated vorinostat,[4] alone or in combination with conventional compounds, to fight various types of cancers. A transcriptomic study revealed that vorinostat modifies the expression of 40% of all genes in cells, explaining, at least in part, the side effects observed with it.[5] Indeed, if vorinostat can be tolerated up to 200 mg/kg in mice, the safe, usual dosing is 50 mg/kg. In humans, safe dosing is up to 300 mg/kg. Like many other chemotherapeutics, vorinostat is rapidly metabolized[6] in vivo by glucuronidation[7] as well as oxidative degradation of the alkyl chain to 4-anilino-4-oxobutanoic acid,[8] and induced resistance to it has been described,[9] all leading to poor results in the clinic.

To improve the therapeutic index of vorinostat, delivery strategies can be used.[10,11] The advantages of drug delivery systems (DDS) are well-established: they can be used to prolong the half-life of the loaded compounds, to develop multitherapies, to help circumvent resistance by bypassing the efflux pumps, to target a specific cancer cell type through their

Received: September 8, 2014
Revised: October 17, 2014
Published: October 21, 2014

modification, and finally to deliver compounds inside cells via endocytosis[12] by exploiting pH variations for release.[13] They can also be designed to achieve passive tumor targeting due to the enhanced permeability and retention effect observed in tumor tissue that does not exist in normal tissues.[14] Several epigenetic inhibitors have thus been delivered by various means.[15] Vorinostat was combined with cyclodextrin in drinking water for brain delivery in mice.[16] By this approach, 200 mg/kg of vorinostat can be dissolved, a dose required for detecting histone reacetylation in brain and spleen, but with some toxicity, limiting its effective delivery to 0.67 g/L (100 mg/kg in mice). Poly(ethylene oxide) (PEO)−polylactic acid (PLA) copolymer micelles[17] improved vorinostat solubility 40-fold. When used with intravenous (i.v.) injection in rats at 10−50 mg/kg, this latter study showed a broad biodistribution of vorinostat, particularly in liver, but no data on its impact on histone acetylation. In these studies, toxicity toward other organs was not discussed.

To date, in vivo models for HDACi delivery are lacking fluorescent reporters that are useful for biodistribution studies, particularly for epigenetic DDS strategies that have not been fully developed. If several cancer cell models are available for in vivo studies, then focusing on cancers with poor prognosis or inefficient care should be considered. Finding solutions for such hard cases could, in turn, also result in better solutions for other types of cancer. Malignant mesothelioma (MM) is a form of lung cancer caused by asbestos exposure.[18] The first-line therapy for MM is a combination of pemetrexed and cisplatin, leading to increased survival of only a few months, and all other single or combined treatments tested also failed with free or delivered molecules. Recent clinical studies on MM suggested that an epigenetic-based approach, eventually used in combination therapy, could be valuable.[19] However, whereas vorinostat displays interesting antitumor properties in vitro against MM, it failed in phase III trials (unpublished, http://goo.gl/dZCFx), probably due to its poor pharmacokinetics properties.

We hypothesized that a pH-responsive DDS for vorinostat could improve its delivery in MM tumors and cells by passive targeting and endocytosis and could contribute to the development of an innovative strategy for this poor-prognosis cancer. This could lead to efficient histone reacetylation in vivo by HDAC inhibition that could possibly impact tumor progression. The rational for this strategy is based on the endocytosis pathway in which acidic vesicles are formed, with pH values ranging from 6 (endosomes) to 5 or less (lysosomes). Designing a pH-responsive prodrug to release bioactive compounds only at a specific pH will ensure that the prodrug should be stable under physiological pH, 7.4, during its blood circulation. If such a prodrug can be linked to nanoparticles able to reach tumors due to an enhanced permeability and retention (EPR) effect and is also able to enter cancer cells via endocytosis, then we can assume that the bioactive compound should be released only at the tumor site and inside cancer cells, avoiding many side effects.

We previously described a pH-responsive prodrug of vorinostat[20] that was found to be stable at physiological pH ($t_{1/2}$ 4 days) with convenient release at pH values below 6 ($t_{1/2}$ 20 h at pH 4) and was also effective in living cells, with restoration of initial HDAC inhibition. As opposed to free vorinostat, which rapidly induced histone reacetylation with a fast decline, our prodrug resulted, in vitro, in a lower amount of reacetylation that was prolonged over time as well as an effective anticancer effect, demonstrating interest in this strategy. This prodrug was designed to contain an alkyne group that could be exploited for click chemistry on azido-bearing nanovectors or macromonomers used to prepare therapeutic nanoparticles. The selection of the delivery system was made by considering two key points. By having the preparation of multifunctional nanoparticles in mind and in order to propose the most straightforward chemistry, we focused our efforts toward preparing already functional macromonomers that could be copolymerized to obtain particles with several functionalities in a controlled ratio. We selected click chemistry as a standardized ligation strategy to prepare functional monomers. Regarding the polymerization method, with the objective being to use our pH-responsive prodrug to be clicked onto the macromonomer prior to polymerization, it was important to select a polymerization reaction that supports functional groups, particularly our pH-sensitive prodrug core. The constrained norbornene bicyclic system has proven to be highly reactive in ring-opening metathesis copolymerization (ROMP) due to the suppression of the cycle tension once the double bond is opened and hence the inability to obtain the reverse reaction, as is known for other monocycloalkenes. Because the metathesis reaction is also a mild process that supports many functional groups, this appeared to be a reasonable choice for developing a novel DDS for the pH-mediated release of vorinostat. In turn, our results with monofunctional macromonomers made of poly(ethylene oxide) (PEO) with norbornene (NB) adapted both to passive targeting and endocytosis[21,22] could be exploited. Indeed, a rhodamine fluorescent version of these nanoparticles (NPs) was selectively accumulated in vivo in tumors by the EPR effect due to the PEO-shell structure of this ROMP-DDS, which introduced native stealth properties. Native cellular internalization was also demonstrated in vitro. Having demonstrated the feasibility of monofunctional nanoparticle synthesis for anticancer applications, we hypothesized that multifunctional copolymers could be made more easily with our generic azidomacromonomer **4** (Scheme 1) that is well-suited for functionalization by click chemistry. Using an alkyne-clickable pH-responsive prodrug of vorinostat[20] and a fluorescent reporter, we envisioned the preparation of a pH-responsive fluorescent (or not) ROMP-DDS from azidomacromonomer **4** and its subsequent use in a mouse model of mesothelioma.

2. MATERIALS AND METHODS

2.1. Materials. Ethanol (96%, purissium grade pur, Xilab), dichloromethane (96%, purissium grade pur, Xilab), and dimethylformamide (DMF, 99.8%, Panreac) were degassed before use. Tetrahydrofuran (THF, J.T. Baker), diethyl ether anhydrous (J.T. Baker), *N*,*N*,*N*′,*N*″,*N*″-pentamethyldiethylenetriamine (PMDETA, 99%, Aldrich), Na_2SO_4 (99%, Alfa Aesar), norbornene (99% GC, Aldrich), Grubbs first-generation catalyst $Cl_2(PCy_3)_2Ru{=}CHPh$ (Aldrich, stored in a glovebox under an Argon atmosphere), dodecane (99%, Aldrich), triethylamine (TEA, 99%, Acros Organics), ethyl vinyl ether (99% stabilized with ca. 0.1% *N*,*N*-diethylalanine, Alfa Aesar), and trizmabase (99.9%, Aldrich) were used without further purification. CuBr (98%, Aldrich) was purified in acetic acid and stored under an inert atmosphere (glovebox). Macromonomers **3**−**5**, unfunctionalized NPs **10**, and pH-responsive vorinostat prodrug **6** were prepared as previously described.[20,21] Synthesized nanoparticles **8** and **9** were purified by ultrafiltration with a system from Millipore (solvent-resistant stirred cell, model XFUF 047 01) with regenerated cellulose ultrafiltration membranes (NMWL = 10 000), ensuring that residual (macro)monomers were totally eliminated.

2.2. Synthesis of the Vorinostat Prodrug-Functionalized Macromonomer 7 (Scheme 1). Prodrug-functionalized macromonomer **7** was obtained by a Huisgen 1,3-cycloaddition between **4** and **6**. Two-hundred forty nine milligrams of **4** (M_n = 3350 g/mol; n = 7 .5 × 10^{-5} mol; 1 equiv), 92 mg of **6** (M = 726 g/mol; n = 1.2 × 10^{-4} mol; 1.5 equiv), and 35 μL of PMDETA (d = 0.83; M = 173 g/mol; n = 1.8 × 10^{-4} mol; 2 equiv) were dissolved in 4.25 mL of DMF. Then, the mixture was degassed according to the freeze−pump−thaw procedure. Twenty-four milligrams of CuBr (M = 143 g/mol; n = 1.8 × 10^{-4} mol; 2 equiv) was then added under an inert atmosphere (glovebox). The mixture was stirred for 4 days under argon at room temperature. Then, 50 mL of dichloromethane was added to the reaction mixture, and the solution was washed 10 times with 30 mL of water and dried with Na_2SO_4. The solution was filtered, the solvent was evaporated, and the macromonomer was dissolved in 30 mL of THF and precipitated in 200 mL of diethyl ether, filtered, dried under vacuum, and finally lyophilized in dioxane. Macromonomer **7** was stored under argon before use. ^{1}H NMR ($CDCl_3$) δ: 9.49 (s, 1H), 7.78 (s, 1H), 7.64 (s, 1H), 7.48 (m, 2H vorinostat), 7.16 (m, 3H vorinostat + 8H toluyl + $CDCl_3$ signal), 6.05−5.85 (m, 2H), 4.57 (s, 2H), 4.43 (m, 4H), 3.76 (m, 4H), 3.57 (m, 312H), 3.32−2.68 (m, NB signals), 2.22 (s, 8H (2H vorinostat)), 2.0−0.25 (m, 10H vorinostat + NB signals); SEC (THF): (RI) M_n = 3690 g/mol (styrene equiv); PDI = 1.18. The functionalization yield was determined by using the ratio between integration of the ethylenic protons and the integration of the proton of the formed triazole ring; F = 80%,

2.3. Synthesis of Nanoparticles 8 (Scheme 1). NPs **8** were obtained by ring-opening-metathesis copolymerization of norbornene **2** with macromonomers **3** and **7** in dispersion. Solvents were degassed according to the freeze−pump−thaw procedure. The reaction was carried out at room temperature under an inert atmosphere (glovebox). In a typical experiment, 10 mg (n = 1.2 × 10^{-5} mol) of Grubbs first-generation complex was dissolved in 5 mL of a dichloromethane/ethanol mixture (50:50 v/v). Both norbornene **2** (0.490 g; M = 94 g/mol; n = 5.2 × 10^{-3} mol) and macromonomers **3** and **7** (m_3 = 0.179 g; $M_{n;3}$ = 3450 g/mol; m_7 = 0.214 g; $M_{n;7}$ = 4125 g/mol; n_3 = n_7 = 5.2 × 10^{-5} mol) were first dissolved in 9 mL of a CH_2Cl_2/EtOH solution (35:65 v/v) (1 mL of this mixture was sampled for analyses) and added to the catalyst solution. NEt_3 (0.1 mL) was added to maintain the pH of the solution above 7. The mixture was stirred for 24 h. At the end of polymerization, ruthenium end-capped chains were deactivated by addition of 0.2 mL of ethyl vinyl ether.

2.4. Synthesis of Nanoparticles 9 (Scheme 1). Grubbs first-generation complex (10 mg; 1.2 × 10^{-5} mol) was dissolved in CH_2Cl_2/EtOH (5 mL; 50:50 v/v). Both norbornene **2** (0.490 g; 5.2 × 10^{-3} mol) and macromonomers **5** (242 mg; 4660 g/mol; 5.2 × 10^{-5} mol) and **7** (214 mg; 4125 g/mol; 5.2 × 10^{-5} mol) were first dissolved in CH_2Cl_2/EtOH (9 mL; 35:65 v/v). Eight milliliters of the latter solution was added to the catalyst solution (1 mL was sampled for analyses). NEt_3 (0.1 mL) was added to maintain the pH of the solution above 7. The mixture was stirred for 24 h. At the end of polymerization, ruthenium end-capped chains were deactivated by addition of 0.3 mL of ethyl vinyl ether. Synthesized nanoparticles **9** were purified by ultrafiltration, ensuring that residual macromonomers **5** and **7** were totally eliminated.

2.5. Macromonomers and Polymers Analysis (Scheme 1 and Figures 1 and 2). ^{1}H NMR studies were completed via a Bruker spectrometer (400 MHz, in $CDCl_3$ at 25 °C). Size-exclusion chromatography (SEC) equipment consists of a JASCO HPLC 880-PU pump, TosoHaas TSK gel columns, a Varian refractive index detector, and a JASCO 875 UV−vis absorption detector, with THF as the mobile phase. The calibration curve was performed using polystyrene standards. The conversion of macromonomers was determined by SEC with dodecane as internal standard (SEC retention times: $t^{SEC}_{macromonomers}$ = 18.75 min; $t^{SEC}_{dodecane}$ = 31.70 min). The conversion of NB was determined by gas chromatography with dodecane as internal standard with a Varian 3900 apparatus having a Factor Four Capillary Column VF-1 ms 15 m × 0.25 mm i.d. DF = 0.25 (injector, T = 250 °C; oven: initial temperature, 50 °C during 2 min followed by a temperature rate of 10 °C/min until 250 °C; detector, T = 300 °C; GC retention times, t^{GC}_{Nb} = 1.77 min and $t^{GC}_{dodecane}$ = 8.55 min). DLS measurements were performed using a MALVERN Zetasizer Nano ZS equipped with He−Ne laser (4 mW and 633 nm). Before measurements, latexes were diluted about 800 times to minimize multiple scatterings caused by high concentration. The scattering angle used was 173°.

2.6. Cell Culture. The pleural mesothelial cell line, MeT-5A, was obtained from the American Type Culture Collection (ATCC). The mesothelioma cell lines Meso13, Meso34, and Meso56 were established from the pleural fluids of mesothelioma patients. All cell lines were maintained in RPMI medium (Invitrogen) supplemented with 2 mM L-glutamine, 100 IU/mL penicillin, 0.1 mg/mL streptomycin, and 10% heat-inactivated fetal calf serum (FCS) (Eurobio).

2.7. Transfections Studies. MeT-5A cells were seeded at a density of 1.5 × 10^5 cells per 35 mm dish. Transient transfections were performed 1 day later using Attractene (Qiagen) according to the manufacturer's protocol. For BRET experiments, MeT-5A cells were transfected with 0.6 μg of Rluc-Brd cDNA and 1 μg of YFP-fused histone H3 cDNA.[23] One day after transfection, cells were transferred into 96-well microplates (microplate 96 well, white, Berthold Technologies) at a density of 3 × 10^4 cells per dish in 180 μL of culture medium. Treatments were performed by the addition of 20 μL of a 10-fold concentrated sample solution. BRET measurements were performed as described below.

2.8. BRET Measurements (Figure 3). All BRET measurements were performed at room temperature using the Mithras LB 940 microplate analyzer (Berthold Technologies). Cells were preincubated for 15 min in PBS in the presence of 2.5 μM coelenterazine (Interchim), following which light-emission acquisition at 485 and 530 nm was carried out. Plates were measured five times. The BRET signal was expressed in milliBRET units (mBu). The BRET unit has been defined previously as the ratio 530/485 nm obtained when the two partners are present, corrected by the ratio 530/485 nm obtained under the same experimental conditions when only the partner fused to *Renilla* luciferase is present in the assay.

2.9. Determination of Cell Viability (Figure 4). Cell growth was monitored using Uptiblue reagent (Interchim). Reduction of this compound by the cell results in the formation of a fluorescent compound quantified by measuring fluorescence at 595 nm after excitation at 532 nm using a Typhoon apparatus (GE Healthcare). Cells were seeded in 96-well plates at a density of 5 × 10^3 cells/well in culture medium. Twenty-four hours later, compound solutions or nanoparticles were added for 72 h. Uptiblue (5%, v/v) was then added to the culture medium for 2 h at 37 °C. Fluorescence was quantified by measuring emission at 595 nm after excitation at 532 nm using a Typhoon apparatus (GE Healthcare).

2.10. Detection of Apoptosis (Figure 4). Apoptosis was quantified using the Annexin V−allophycocyanin (APC) apoptosis detection kit (Becton Dickinson), which labels phosphatidylserine externalized in the early phases of apoptosis. Cells were seeded at a density of 1 × 10^5 per well of 6-well plates and treated with NPs **10** at 1 mg/mL or NPs **8** at 1 mg/mL (45 μM vorinostat). After 48 h of culture, floating and adherent cells were combined, washed twice with cold PBS, resuspended in 100 μL of annexin binding buffer (10 mmol/L Hepes, 140 mmol/L NaCl, 2.5 mmol/L $CaCl_2$, pH 7.4), incubated for 15 min at room temperature with 2.5 μL of Annexin V−FITC and 2.5 μL of propidium iodide, and analyzed by flow cytometry (FACSCalibur; Becton Dickinson). Ten thousand events were collected and analyzed with FACS Flowjo Software.

2.11. Animal Experiments (Figures 5 and S3). These experiments were carried out in compliance with the guidelines of the European Union for the care and use of animals in research protocols. The experiments were approved by ethical committee for animal experiment (CEEA.PdL 2013.6).

2.11.1. Biodistribution Experiments. Three million AK7 murine mesothelioma cells (AK7) per mouse were administered subcutaneously in the hind leg of five nude mice (CD-1, Charles River) (day 0). Mice were given six successive i.v. injections of NPs **9** (160 mg/

Scheme 1. Macromonomers and Copolymers Syntheses[a]

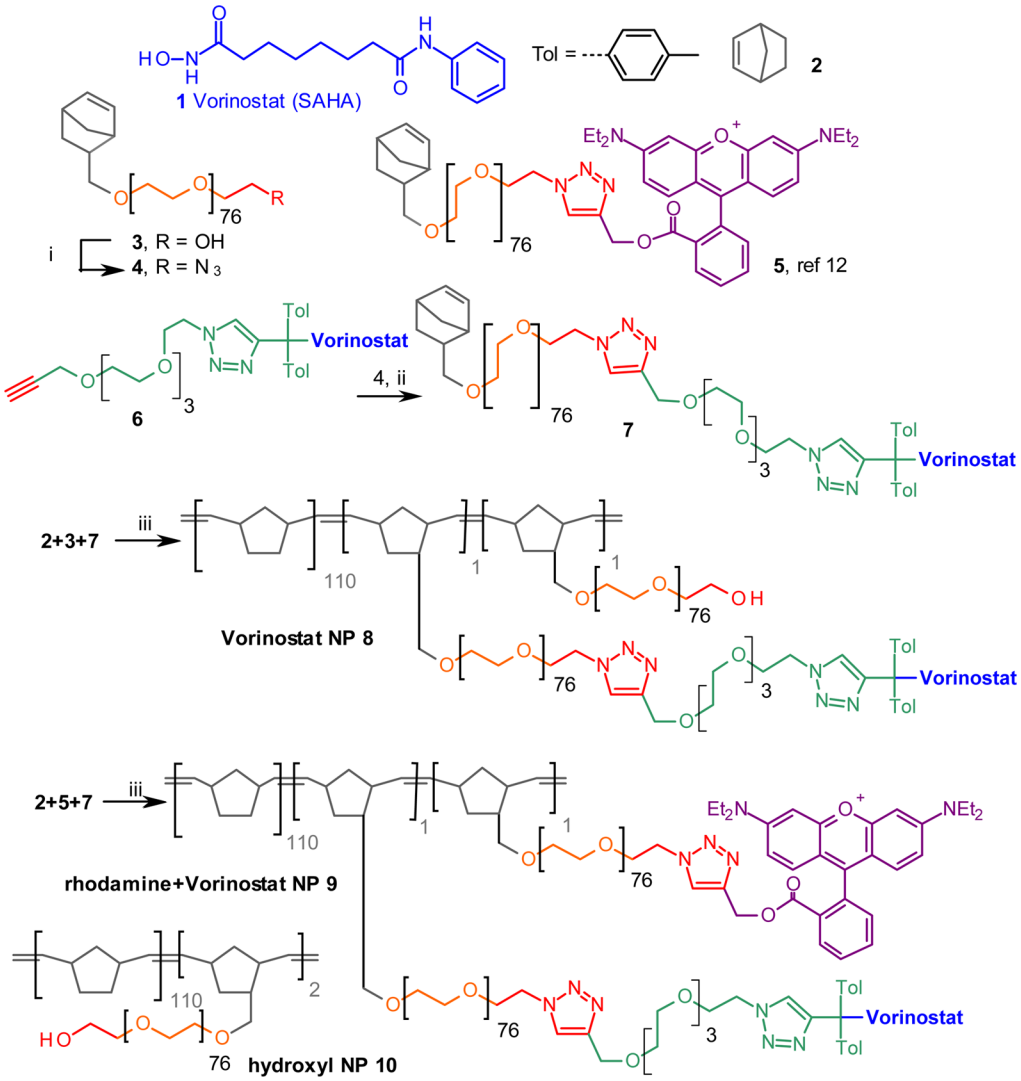

[a](i) (a) MsCl; (b) NaN_3 (ii) CuBr, PMDETA; (iii) Grubbs I; EtOH/CH_2Cl_2, TEA.

kg), respectively, at days 14, 16, 19, 21, 23, and 26. All animals were necropsied on days 28/29. Tumor, liver, ovary, brain, spleen, and kidneys were collected and analyzed for fluorescence emission. Fluorescence was observed at 630 nm using Photon Imager (Biospace Lab) after excitation at 580 nm, and pictures were analyzed using PhotoVision+ software (Biospace Lab).

*2.11.2. In Vivo Activity of Nanoparticles **8** and **10**.* Three million AK7 murine mesothelioma cells (AK7) per mouse were administered subcutaneously in the hind leg of three groups of five nude mice (CD-1, Charles River) (day 0). Group 1 did not receive any further treatment. Groups 2−4 were, respectively, given six successive i.v. injections of vorinostat (50 mg/kg), NPs **10** (160 mg/kg), or NPs **8** (160 mg/kg, 1.9 mg/kg vorinostat equivalent) at days 14, 16, 19, 21, 23, and 26. All animals were necropsied on days 28/29. Mice, liver, kidneys, and spleen were weighed. Blood analyses, using a MS9-5 analyzer (Melet Schloesing laboratories), were performed, and tumors were collected to perform immunohistochemical analyses.

2.12. Immunohistochemistry (Figure 6). Tumors were fixed in 4% CH_2O in PBS, embedded in paraffin, and sectioned into 5 μm sections. Immunohistochemistry was performed on tumor slices (paraffin-embedded) by the Cellular and Tissular Imaging Core Facility of Nantes University (MicroPICell) using standard techniques. The primary antibodies used were anti-activated caspase 3 (Abcam) and anti-histone H3 acetyl (specific to acetylated lysines 9, 14, 18, 23, and 27) (Active motif) as recommended by the manufacturers. N-Histofine Simple Stain Mouse MAX Peroxidase (Nichirei Biosciences, Tokyo, Japan) was used as the detection reagent. Pictures were obtained using a NanoZoomer 2.0HT (Hamamatsu).

3. RESULTS AND DISCUSSION

3.1. Preparation and Characterization of Macromonomer 7. This article presents the development of NPs **8** (Scheme 1) as a DDS for vorinostat as well as the determination of its biological activities in vitro and in vivo. Fluorescent copolymer **9** was also prepared to demonstrate (i) that multifunctional NPs can be prepared with a controlled ratio of functionalities and (ii) that combining the fluorescent macromonomer **5** and the pH-responsive vorinostat macromonomer **7** does not modify the biodistribution in vivo compared to that of NPs prepared with macromonomer **5** only.[21] Macromonomer **7** (Scheme 1) was prepared by click chemistry between alkyne prodrug **6** and macromonomer **4**[22] prepared with average PEO length n = 76. The clickable prodrug **6** was best suited for the release of vorinostat under mildly acidic pH with convenient stability at physiological pH[20] to avoid the release of active molecule in blood vessels.

dx.doi.org/10.1021/bm501338r | *Biomacromolecules* 2014, 15, 4534−4543

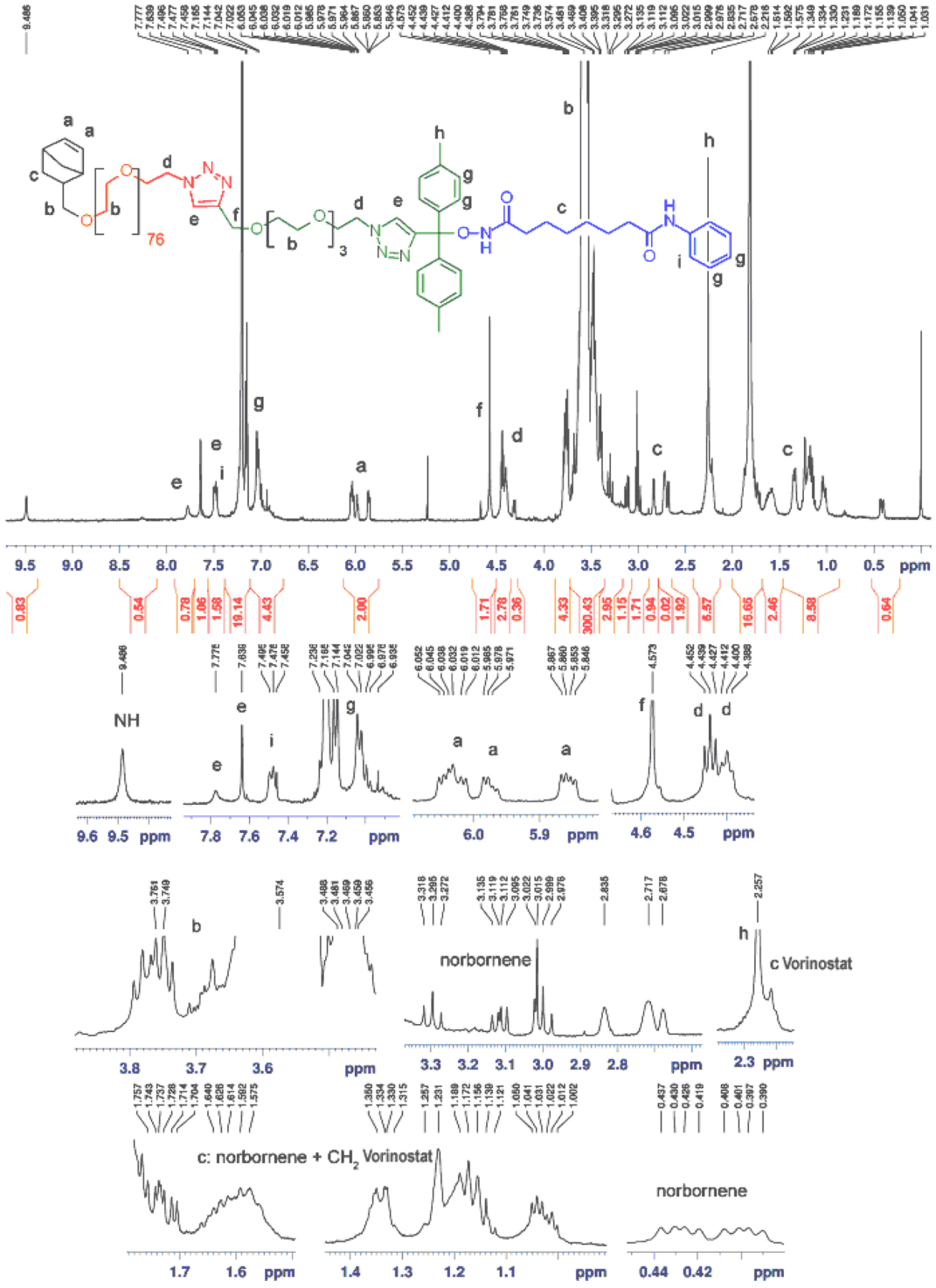

Figure 1. ^{1}H NMR characterization of triazole macromonomer **7**.

Using copper catalyzed Huisgen cycloaddition in the presence of PMDETA as copper ligand, azide **4** reacted with alkyne **6** to give triazole macromonomers **7** in good yields (80%, Supporting Information for characterization), determined using the ratio between the integration of ethylenic protons a (Figure 1) and integration of proton e of the formed triazole ring on the ^{1}H NMR spectra. Chemical shifts were attributed by comparison to starting materials (Figure S1, Supporting Information).

3.2. Preparation and Characterization of Nanoparticles 8 and 9. Combinations of NB + **3** + **7** gave access to vorinostat functional NPs **8**, whereas difunctional rhodamine + vorinostat prodrug NPs **9** were prepared by combining NB, **7**, and the fluorescent macromonomer **5**[21] (Scheme 1). The general protocol for the synthesis of NPs **8** and **9** by ROMP with Grubbs I catalyst in dispersed media involved NB (100 equiv) and macromonomer **7** (1 equiv) mixed with macromonomers **3** (for NP **8**, 1 equiv) or **5** (for NP **9**, 1 equiv). We used the same amount of vorinostat−macromonomer **7** in the

dx.doi.org/10.1021/bm501338r | *Biomacromolecules* 2014, 15, 4534−4543

syntheses of both NPs **8** and **9** to allow for comparative studies in vitro and in vivo. For all NP batches, NB and macromonomer conversions were determined by gas chromatography and size-exclusion chromatography,respectively, and, in each case, provided conversions higher than 99% for NB and higher than 90% for the macromonomers (Figure S1 and calculations, Supporting Information).

Regarding the initial amounts of monomer and macromonomers and their conversions, we determined that the final latexes were composed of polymerized chains in a ratio 110:1:1 for the (macro)monomer units **2**:**7**:(**3** or **5**) (Table S1, Supporting Information). For biological purposes, these NPs were transferred in aqueous solutions, carried out by successive evaporation and purification by ultrafiltration,[21] by diluting the dispersion in order to obtain a polymer concentration of 20 mg/mL (0.9 μM of vorinostat). All of these nanoparticles were then characterized by DLS in order to confirm their colloidal stabilities (Figure 2) and to determine their sizes in the reaction

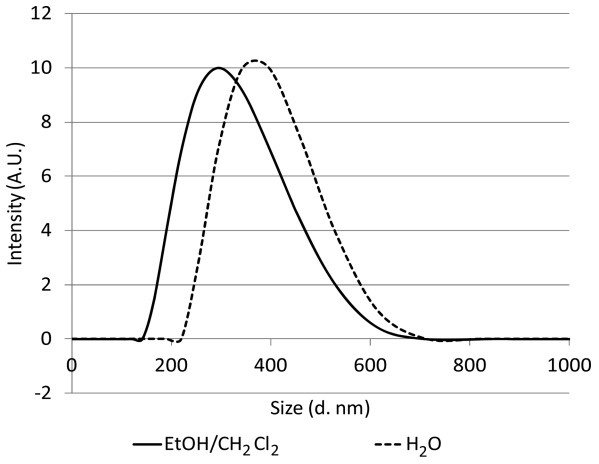

Figure 2. DLS measurement of nanoparticles **8** dispersed in EtOH/CH_2Cl_2 mixture and in water.

medium and in water after their transfer (Table S1). Figure 2 shows that the initial size of the particles synthesized in a EtOH/CH_2Cl_2 mixture is close to 300 nm and that the transfer in water slightly improved the distribution and the size was slightly bigger, probably due to water molecule inclusion in the hydrophilic PEO shell.

The hydroxyl NPs **10**[21] (Scheme 1) were used as negative controls in biological experiments. In the clinic, the dose-limiting toxicity for vorinostat is below 300 mg/day (about 1 mmol). This suggests that our NPs with 1% vorinostat loading should be used at a maximum of 100 mmol/day to obtain the same amount of free vorinostat. Taking into account the fast metabolism of vorinostat in vivo (<2 h), we hypothesized that using such NPs should help to optimize vorinostat delivery for a higher local effect, allowing reduced vorinostat dosing and, in turn, reduced toxicity.

3.3. HDAC Inhibition with Nanoparticles 8 and 9. With vorinostat-bearing NPs **8** (Scheme 1), we first investigated the restoration of HDAC inhibition with a bioluminescent resonance energy transfer (BRET) assay[23] designed to measure histone H3 acetylation in living cells (Figure 3). When performed with living cells, this assay can also confirm cellular internalization of the NPs. Dose-dependent BRET induction experiments were performed on cells treated for 16 h with vorinostat and NPs **8** and **10** to determine their pharmacological properties (Figure 3A,B). Vorinostat-bearing NPs **8** were compared to hydroxyl NPs **10** as a vorinostat-negative control and free vorinostat as a positive control. As expected, NPs **8** triggered dose-dependent BRET signal induction and then a dose-dependent increase of histone H3 acetylation, whereas the NPs **10** negative control gave no significant signal (Figure 3A). NPs **8** doses higher than 22.5 μM of vorinostat equivalents (500 μg/mL of polymer) led to a reduction of BRET signal, which likely corresponds to an intrinsic effect of the NPs on the cells, suggesting a safe window below 500 μg/mL polymer concentration for experiments on cells in culture. Vorinostat gave enhanced BRET signal induction (Figure 3B, 273.22 $\pm$ 44.66 mBu), which was five times higher than that of NPs **8** (61.11 $\pm$ 7.26 mBu).

BRET induction kinetics at IC_{50} concentrations (Figure 3C,D, 5 μM vorinostat and 0.25 mg/mL NPs **8** = 11.25 μM vorinostat) showed a fast response for vorinostat, which was rapidly delivered in cells by diffusion, with a maximum BRET induction at 20 h, followed by a rapid signal reduction. In contrast, NPs **8** triggered a lower, delayed (40 h), and continuous BRET signal induction, suggesting two cellular events required for thier HDAC inhibition: cellular internalization and vorinostat release. Under kinetic conditions, vorinostat alone gave 2-fold more BRET induction than that of vorinostat-bearing NPs (Figure 3E, 331.88 $\pm$ 22.79 mBu for vorinostat and 158.73 $\pm$ 9.71 mBu for NPs **8**). The same kinetics were previously obtained for prodrug **6**,[22] demonstrating that once grafted onto NPs, the release of vorinostat from the pH-responsive system in living cells is not modified.

This common BRET profile revealed that the fast vorinostat metabolism (<2 h) when used alone is overcome due to the high concentration reached within the cells after one shot, leading to high and transient histone H3 acetylation. In contrast, NPs **8** allow equilibrium to be reached between vorinostat release and its metabolic consumption, resulting in the presence of a relatively constant vorinostat concentration in cells after 24 h and then to a moderate and constant histone H3 acetylation over time. The kinetics obtained for NPs **8** was analyzed by visualization of the internalization of their fluorescent counterpart, **9** (Figure S2, Supporting Information). Multilayer analysis of MPM cells treated with fluorescent NPs **9** clearly showed internalization (red dots) in cells around the nucleus (blue), with the first signal appearing at 8 h and a higher amount after 24 h. This internalization process is consistent with the observed maximum BRET signal at 20 h.

3.4. Viability of Cells Treated with Nanoparticles 8 and 10. Viability experiments (Figure 4A,B) demonstrated an absence of hydroxyl NPs **10** toxicity toward cells, whereas the same polymer concentrations of vorinostat NPs **8** significantly decreased cancer cell viability in a dose-dependent manner (Figure 4A). When compared to the toxicity of free vorinostat, NPs **8** toxicity was lower (Figure 4B), a result consistent with BRET experiments (Figure 3) and thus correlated to the level of histone H3 acetylation.

Indeed, vorinostat was toxic in our cell model at 10 μM, at which concentration no cells were viable, whereas at least 50% of cells remained alive with vorinostat NPs **8** at 100 μM of equivalent vorinostat. HDAC inhibition is correlated with apoptosis in cancer cell lines, confirmed in our case by annexin V staining, whereas, as expected, hydroxyl NPs **10** triggered no apoptosis. NPs **8** at 45 μM of equivalent vorinostat (1 mg/mL polymer) gave a dramatic increase of apoptosis at 48 h, which was even higher after 72 h (Figure 4C,D). This was correlated

dx.doi.org/10.1021/bm501338r | *Biomacromolecules* 2014, 15, 4534−4543

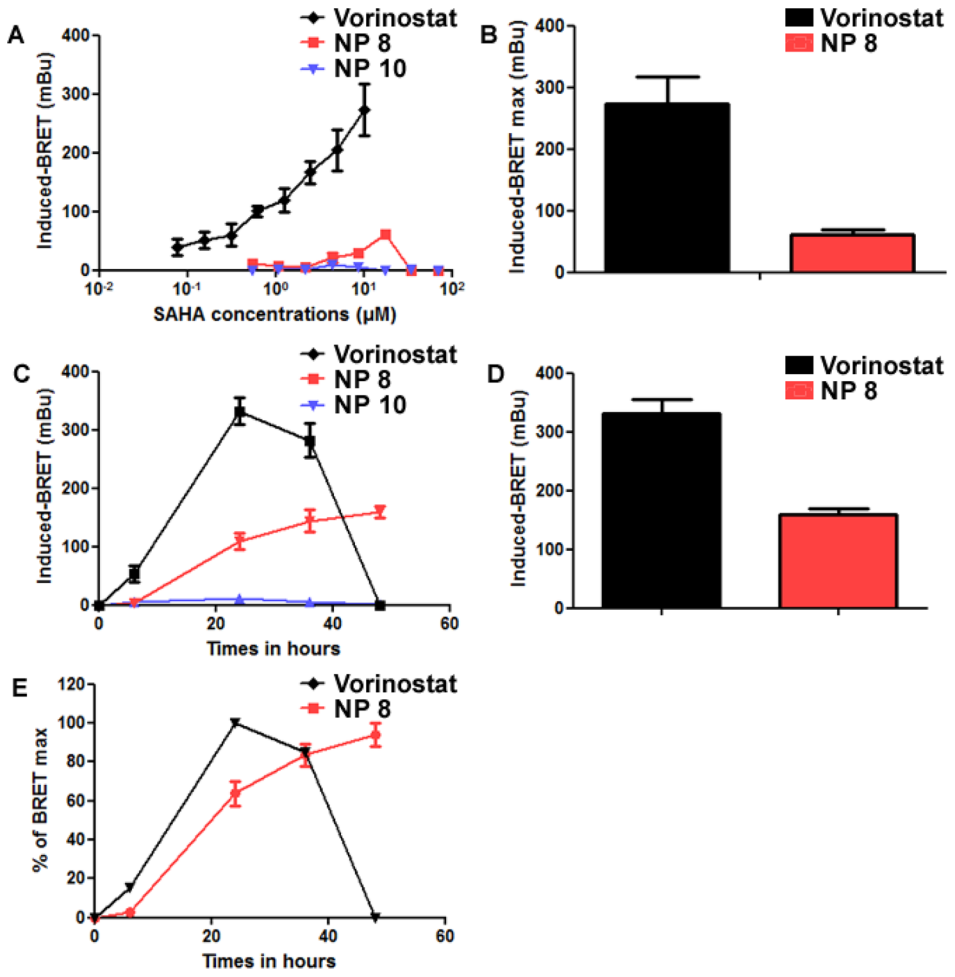

Figure 3. Pharmacological characterization of nanoparticles **8**, **10**, and vorinostat using BRET. MeT-5A cells were transfected with phRluc-C1 BrD and pEYFP-C1 histone H3. (A) Cells were treated for 16 h with increasing doses of the different molecules. (B) Graphic represents the maximal induced BRET signal measured for each molecule in the dose−response experiment. (C, E) Cells were treated with 5 μM vorinostat or 0.25 mg/mL NPs **8** (11.25 μM vorinostat) for 8, 24, 36, or 48 h. (C) Results are expressed as the induced BRET signal. (D) Maximal induced BRET signal measured for each molecule independently of the time of treatment. (E) Percent of the maximal induced BRET signal measured during kinetic experiments. Results are the mean ± SEM of three independent experiments.

with the delayed release of vorinostat from NPs **8** and was consistent with previous effects obtained on histone H3 acetylation and cell viability. Regarding our results, we can confirm that our NPs were internalized by cells and that, subsequently, these NPs should traffic through the endosomal/lysosomal pathways where the increased acidity can be exploited to release vorinostat in a pH-dependent manner. The functionality of our NPs in vitro warranted further investigation in vivo to validate a possible effect in tumors by exploiting the enhanced permeability and retention effect.[14]

3.5. In Vivo Effects of Nanoparticles 8−10. We previously demonstrated, through biodistribution studies with a fluorescent version of our NPs conducted in mice, that such NPs accumulate mainly within the tumor.[22] Here, we first confirmed that the introduction of the pH-responsive form of vorinostat covalently linked to fluorescent NPs did not modify the behavior of the NPs in vivo. Therefore, mice bearing subcutaneous tumors were injected intravenously with 160 mg/kg of rhodamine + vorinostat NPs **9** (schedule in Figure S3, Supporting Information). All mice survived after treatment and were euthanized for tumor collection and analysis of biodistribution by fluorescent imaging. Figure 5A,B shows that NPs **9** were also mainly accumulated in the tumor, whereas no NPs **9** were detected in liver, kidneys, brain, and ovaries, as demonstrated by the absence of a change in the fluorescent signal between organs from untreated mice and NPs **9** injected mice (Figure 5B) (all mouse pictures are provided in Supporting Information Figure S4).

Taking into account that rhodamine + vorinostat NPs **9** showed the same biodistribution as that of rhodamine-only NPs[22] and that the fluorescent probe was not expected to change the biodistribution, NPs **8** and **10** and free vorinostat were compared in vivo. MM tumor cells were injected in 4 groups, each composed of 5 mice, corresponding to (1) a control group that was not treated and groups treated with (2) vorinostat, (3) hydroxyl NPs **10**, and (4) vorinostat NPs **8** (the schedule for this experiment is in Figure S3). Activated caspase-3 staining did not reveal a higher amount of apoptotic area in the tumors of mice treated with NPs **8** compared to that in untreated mice, vorinostat, or NPs **10** treated mice (Figure 6, top row).

However, global histone H3 acetylation was clearly increased in tumors of NPs **8** treated mice (brown labeled cell nuclei) (Figure 6, bottom row; for all mice, see Figure S5, Supporting Information) compared to that in untreated, vorinostat, or NPs **10** treated mice. This effect was obtained in which the

dx.doi.org/10.1021/bm501338r | *Biomacromolecules* 2014, 15, 4534−4543

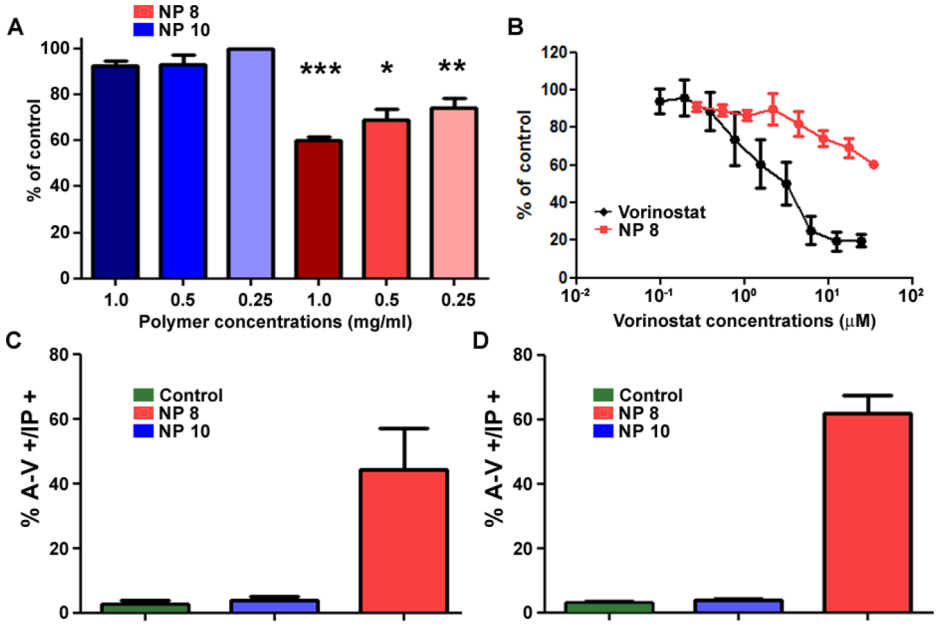

Figure 4. Biological characterization of NPs and vorinostat. Viability of MM cells was evaluated following treatments with increasing amounts of hydroxyl NPs **10** (A), vorinostat NPs **8** (A, B), or vorinostat (B) for 72 h. MM cells were treated with 1 mg/mL of NPs **10** or **8** (45 μM vorinostat; 1 mg/mL polymer) for 48 h (C) or 72 h (D), and apoptosis induction was measured by annexin V−APC labeling. Results are the mean ± SEM of three independent experiments. *, $p < 0.05$; **, $p < 0.01$; and ***, $p < 0.001$.

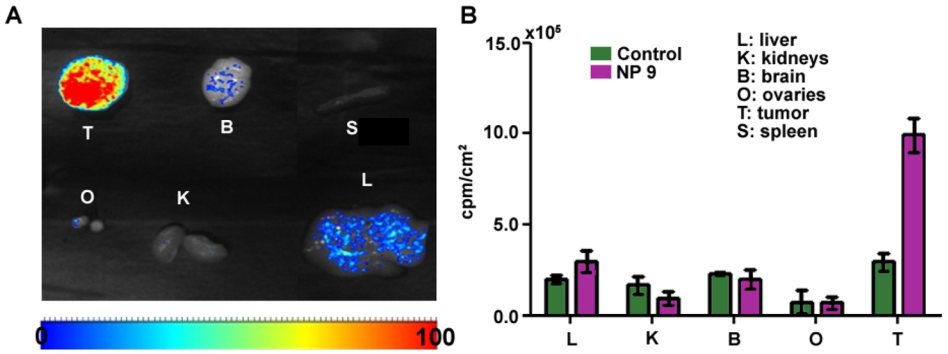

Figure 5. Biodistribution of NPs **9** in a mouse model of subcutaneous mesothelioma. Nude mice bearing AK7 tumors were injected with 160 mg/kg of NPs **9** in the tail vein. (A) Representative picture of fluorescence observed on dissected tumor (T), liver (L), ovary (O), brain (B), spleen (S), and kidneys (K). (B) Quantification of NPs **9** biodistribution. Results are the mean ± SEM from 5 mice.

equivalent amounts of injected vorinostat NPs **8** (1.9 mg/kg) were more than 25-fold lower than those of free vorinostat (50 mg/kg). The absence of major apoptosis induction by NPs **8** and the increase of histone H3 acetylation suggest that vorinostat doses delivered into the tumor could be sufficient to increase tumor suppressor gene expression and then sensitize cells to other drugs.

3.6. In Vivo Toxicity of Nanoparticles 8 and 10. In order to detect an eventual toxicity of the treatments, blood samples were collected, blood was analyzed, and the mouse as well as its liver, spleen, and kidneys was weighed. Comparing all groups, no variation in the levels of erythrocytes, thrombocytes, and leucocytes was observed, nor was there any variation in the weight of mice and of the different organs (Figure S6 and S7, Supporting Information).

4. CONCLUSIONS

Vorinostat is currently approved for the treatment of cutaneous T-cell lymphoma, but, to date, it has not given satisfactory results against solid and diffuse tumors, particularly for MM. The poor solubility, fast metabolism, and high toxicity of vorinostat, notably, thrombopenia, are responsible for its limited dosing in the clinic (DLT 300−400 mg/day). Improving vorinostat delivery in solid tumors in vivo was made possible through a pH-responsive DDS able to passively target tumors with subsequent cellular internalization independent of receptor-mediated endocytosis. Following internalization, the inhibitor is slowly released in cells, avoiding potential side effects arising from diffusion outside the tumoral zone. This strategy should limit the clearance and metabolism of vorinostat and yield better clinical results. Our pH-responsive DDS, easily produced by ROMP, appears to be a good strategy to increase vorinostat-induced acetylation in solid tumors. Such tools can be used to decipher chromatin reacetylation effects in vivo as an entry to better understanding the in vivo chemical biology of HDAC inhibitors and, by extension, other chromatin-modifying enzyme inhibitors. This reacetylation is also an entry point to sensitize malignant cells to other anticancer drugs, and such an epigenetic strategy is currently being investigated. Thus, this could lead to a decrease

dx.doi.org/10.1021/bm501338r | *Biomacromolecules* 2014, 15, 4534−4543

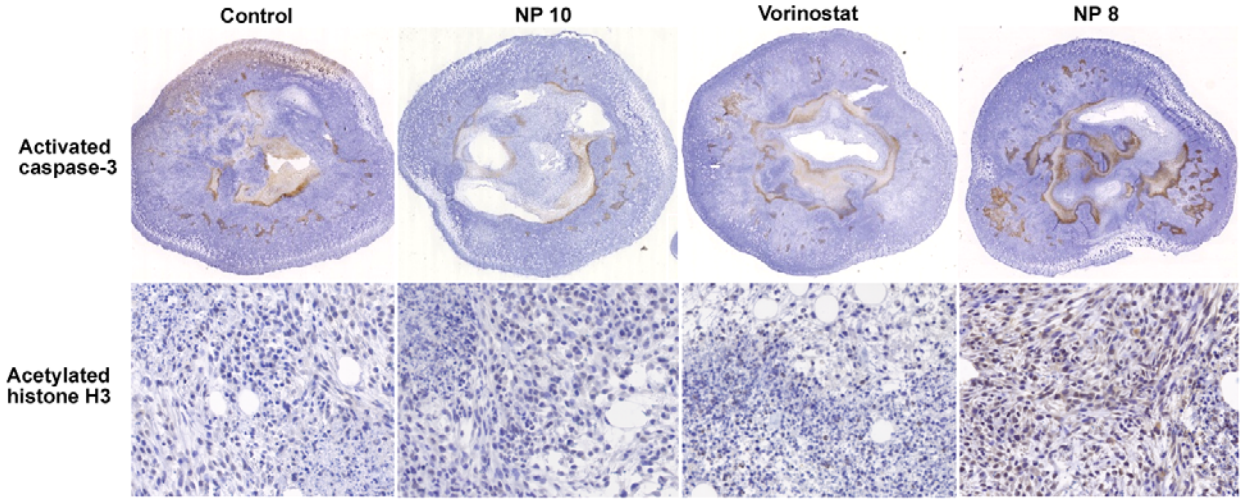

Figure 6. Tumors were analyzed by immunohistochemistry using anti-activated caspase-3 or anti-acetylated histone H3 antibodies. Nude mice bearing subcutaneous AK7 tumors were treated with intravenous injection of hydroxyl NPs **10** (160 mg/kg), vorinostat (50 mg/kg), or vorinostat NPs **8** (1.9 mg/kg vorinostat, 160 mg/kg polymer).

of the doses currently administered in clinical trials and to an increase of their therapeutic benefit.

■ ASSOCIATED CONTENT

Ⓢ Supporting Information

^{1}H NMR spectra of reference intermediates, details of the characterization of macromonomers, calculations for the composition of new nanoparticles, details of the in vivo schedule, and toxicological assessments of the effects of NPs and vorinostat in all groups of mice. This material is available free of charge via the Internet at http://pubs.acs.org.

■ AUTHOR INFORMATION

Corresponding Authors

*(P.B.) E-mail: philippe.bertrand@univ-poitiers.fr; Tel.: (+33) (0)549454192; Fax: (+33) (0)549453502.

*(C.B.) E-mail: christophe.blanquart@inserm.fr; Tel.: (+33) (0)228080238; Fax: (+33)(0)220080204.

Author Contributions

All authors contributed equally to this work.

Notes

The authors declare no competing financial interest.

■ ACKNOWLEDGMENTS

We thank the Agence Nationale de la Recherche (ANR) for grants to R.D., F.G., and F.C. (ANR-08-PCVI-030); Région Poitou-Charentes for a grant to F.E.B., the Ligue National Contre la Cancer for a grant to I.D.; the Ligue Contre le Cancer: committees of Morbihan, Sarthe, Vendée, Loire-Atlantique et Charente-Maritime, Centre National de la Recherche Scientifique (CNRS), ARSMESO44, Nantes University Hospital, and COST action TD0905.

■ REFERENCES

(1) Duvic, M.; Vu, J. *Expert Opin. Invest. Drugs* **2007**, *16*, 1111.

(2) Richon, V. M.; Webb, Y.; Merger, R.; Sheppard, T.; Jursic, B.; Ngo, L.; Civoli, F.; Breslow, R.; Rifkind, R. A.; Marks, P. A. *Proc. Natl. Acad. Sci. U.S.A.* **1996**, *93*, 5705.

(3) Butler, L. M.; Agus, D. B.; Scher, H. L.; Higgins, B.; Rose, A.; Cordon-Cardo, C.; Thaler, H. T. R.; Rifkind, A.; Marks, P. A.; Richon, V. M. *Cancer Res.* **2000**, *60*, 5165.

(4) Martinet, N.; Bertrand, P. *Cancer Manag. Res.* **2011**, *3*, 117.

(5) Peart, M. J.; Smyth, G. K.; Rvan Laar, K.; Bowtell, D. D.; Richon, V. M.; Marks, P. A.; Holloway, A. J.; Johnstone, R. W. *Proc. Natl. Acad. Sci. U.S.A.* **2005**, *102*, 3697.

(6) Flipo, M.; Charton, J.; Hocine, A.; Dassonneville, S.; Deprez, B.; Deprez-Poulain, R. *J. Med. Chem.* **2009**, *52*, 6790.

(7) Du, L.; Musson, D. G.; Wang, A. Q. *J. Pharm. Biomed. Anal.* **2006**, *42*, 556.

(8) Parise, R. A.; Holleran, J. L.; Beuner, J. H.; Ramalingam, S.; Egorin, M. J. *J. Chromatogr. B* **2006**, *840*, 108.

(9) Dedes, K. J.; Dedes, I.; Imesch, P.; von Bueren, A. O.; Fink, D.; Fedier, A. *Anticancer Drugs* **2009**, *20*, 321.

(10) Peer, D.; Karp, J. M.; Hong, S.; Farokhzad, O. C.; Margalit, R.; Langer, R. *Nat. Nanotechnol.* **2007**, *2*, 751.

(11) Zhang, L.; Gu, F. X.; Chan, J. M.; Wang, A. Z.; Langer, R. S.; Farokhzad, O. C. *Clin. Pharmacol. Ther.* **2008**, *83*, 761.

(12) Scita, G.; Di Fiore, P. P. *Nature* **2010**, *463*, 464.

(13) Modi, S.; Swetha, M. G.; Goswami, D.; Gupta, G. D.; Mayor, S.; Krishnan, Y. *Nat. Nanotechnol.* **2009**, *4*, 325.

(14) Sato, N. L.; Niimura, S.; Fujisawa, N.; Maeda, Y. *Jpn. J. Pharmacol.* **1986**, *41*, 163.

(15) el Bahhaj, F.; Dekker, F. J.; Martinet, N.; Bertrand, P. *Drug Discovery Today* **2014**, *19*, 1337.

(16) Hockly, E.; Richon, V. M.; Woodman, B.; Smith, D. L.; Zhou, X.; Rosa, E.; Sathasivam, K.; Ghazi-Noori, S.; Mahal, A.; Lowden, P. A.; Steffan, J. S.; Marsh, J. L.; Thompson, L. M.; Lewis, C. M.; Marks, P. A.; Bates, G. P. *Proc. Natl. Acad. Sci. U.S.A.* **2003**, *100*, 2041.

(17) Mohamed, E. A.; Zhao, Y.; Meshali, M. M.; Remsberg, C. M.; Borg, T. M.; Foda, A. M.; Takemoto, J. K.; Sayre, C. L.; Martinez, S. E.; Davies, N. M.; Forrest, M. L. *J. Pharm. Sci.* **2012**, *101*, 3787.

(18) (a) Guillot, F.; Boutin, B.; Blanquart, C.; Fonteneau, J. F.; Robard, M.; Gregoire, M.; Pouliquen, D. *Vaccine* **2011**, *29*, 5534. (b) Barbone, D.; Cheung, P.; Battula, S.; Busacca, S.; Gray, S. G.; Longley, D. B.; Bueno, R.; Sugarbaker, D. J.; Fennell, D. A.; Broaddus, V. C. *PLoS One* **2012**, *7*, e52753. (c) Hurwitz, J. L.; Stasik, I.; Kerr, E. M.; Holohan, C.; Redmond, K. M.; McLaughlin, K. M.; Busacca, S.; Barbone, D.; Broaddus, V. C.; Gray, S. G.; O'Byrne, K. J.; Johnston, P. G.; Fennell, D. A.; Longley, D. B. *Eur. J. Cancer* **2012**, *48*, 1096.

(19) Vandermeers, F.; Sriramareddy, S. N.; Costa, C.; Hubaux, R.; Cosse, J.-P.; Willems, L. *Lung Cancer* **2013**, *81*, 311.

(20) Delatouche, R.; Denis, I.; Grinda, M.; el Bahhaj, F.; Baucher, E.; Collette, F.; Héroguez, V.; Gregoire, M.; Blanquart, C.; Bertrand, P. *Eur. J. Pharm. Biopharm.* **2013**, *85*, 862.

(21) Collette, F.; Delatouche, R.; Blanquart, C.; Gueugnon, F.; Grégoire, M.; Bertrand, P.; Héroguez, V. *J. Polym. Sci., Part A: Polym. Chem.* **2013**, *51*, 176.
(22) Gueugnon, F.; Denis, I.; Pouliquen, D.; Collette, F.; Delatouche, R.; Héroguez, V.; Gregoire, M.; Bertrand, P.; Blanquart, C. *Biomacromolecules* **2013**, *14*, 2396.
(23) Blanquart, C.; Francois, M.; Charrier, C.; Bertrand, P.; Gregoire, M. *Curr. Cancer Drug Targets* **2011**, *11*, 919.